Plasmonic Pumping of Excitonic Photoluminescence in Hybrid MoS_2–Au Nanostructures

Sina Najmaei,[†] Adnen Mlayah,[‡] Arnaud Arbouet,[‡] Christian Girard,[‡] Jean Léotin,[§] and Jun Lou*[,†]

[†]Department of Materials Science and NanoEngineering, Rice University, Houston, Texas 77005, United States, [‡]Centre d'Elaboration de Matériaux et d'Etudes Structurales, UPR 8011, CNRS-Université de Toulouse, 29 Rue Jeanne Marvig, BP 94347, F-31055 Toulouse, France, and [§]Laboratoire National des Champs Magnétiques Intenses, UPR 3228, CNRS-UJF-UPS-INSA, Grenoble and Toulouse, France

ABSTRACT We report on the fabrication of monolayer MoS_2-coated gold nanoantennas combining chemical vapor deposition, e-beam lithography surface patterning, and a soft lift-off/transfer technique. The optical properties of these hybrid plasmonic–excitonic nanostructures are investigated using spatially resolved photoluminescence spectroscopy. Off- and in-resonance plasmonic pumping of the MoS_2 excitonic luminescence showed distinct behaviors. For plasmonically mediated pumping, we found a significant enhancement (~65%) of the photoluminescence intensity, clear evidence that the optical properties of the MoS_2 monolayer are strongly influenced by the nanoantenna surface plasmons. In addition, a systematic photoluminescence broadening and red-shift in nanoantenna locations is observed which is interpreted in terms of plasmonic enhanced optical absorption and subsequent heating of the MoS_2 monolayers. Using a temperature calibration procedure based on photoluminescence spectral characteristics, we were able to estimate the local temperature changes. We found that the plasmonically induced MoS_2 temperature increase is nearly four times larger than in the MoS_2 reference temperatures. This study shines light on the plasmonic–excitonic interaction in these hybrid metal/semiconductor nanostructures and provides a unique approach for the engineering of optoelectronic devices based on the light-to-current conversion.

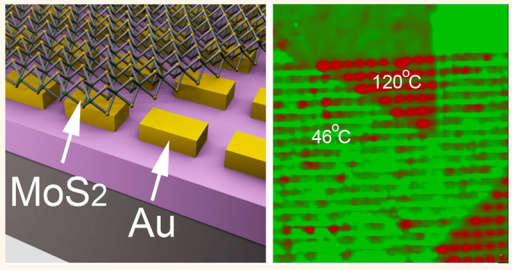

KEYWORDS: plasmonic · photoluminescence · nanostructure

Molybdenum disulfide (MoS_2) monolayers are a semiconducting member of two-dimensional transition metal dichalcogenides with promising physical properties.[1] The unique characteristics of MoS_2 atomic layers show great promise in future optoelectronics.[2] The strong spin–orbit interactions[3] and symmetry properties of this material suggest remarkable spin valley coupling that can be utilized to effectively populate the valley states in the band structure of this material.[4–6] Additionally, the efficient photoemission properties, strong excitonic binding, nonlinear optical response, and chemical stability of MoS_2 has motivated extensive studies to understand its light–matter interactions.[7] However, for applications of this material in optoelectronics, novel approaches to enhance and control its optical response are essential.

One effective approach to enhance and remotely control the optical response of materials relies on the use of localized surface plasmon resonances (LSPR) sustained by metal nanoparticles. Indeed, it has been shown that, using plasmonic resonators, the photocurrent extracted from 2D materials such as MoS_2 can be significantly increased through careful optimization of its light absorption.[7] A primitive nanophotonic integrated circuit composed of a single silver nanowire and MoS_2 flake has been suggested recently.[8] Also recently, it has been shown that hot electrons generated by plasmonic nanoparticles can result in phase transitions in the MoS_2 crystal structure.[9] However, little is known about the near-field interaction between the surface plasmons and the MoS_2 optical transitions. Therefore, understanding the relevant interaction mechanisms in these hybrid systems may provide a unique opportunity for monitoring the optical properties of the 2D dichalcogenide monolayers and for probing their excitonic-plasmonic interactions.

* Address correspondence to jlou@rice.edu.

Received for review October 5, 2014 and accepted December 3, 2014.

Published online December 03, 2014
10.1021/nn5056942

In this work, we report the successful transfer of MoS_2 monolayers, grown by chemical vapor deposition (CVD), to gold nanoantenna fabricated using electron beam (e-beam) lithography, and we investigate the photoluminescence properties of this hybrid system. The MoS_2 monolayer has the great advantage of introducing a well-controlled local absorber (and emitter) in the plasmonic near-field of the gold nanoantenna. This work is focused on the plasmonic mediated pumping of the MoS_2 photoluminescence emission. Off- and in-resonance excitation of the surface plasmons produced drastically different behaviors of the photoluminescence emission from the MoS_2. In particular, adopting a temperature calibration procedure of the MoS_2 PL emission, we were able to measure the temperature elevations in MoS_2 caused by the plasmonic mediated light absorption. Based on green dyadic method[10] (GDM) and Discrete Dipole Approximation (DDA) simulations of the plasmonic properties, combined with heat dissipation calculations, we discuss the contribution of the plasmonically induced heating to the measured temperature increase. We found that the results can be interpreted in terms of absorption of light by the plasmonic nanoantenna and its conversion into electron−hole pair excitations of the 2D MoS_2 monolayer thus leading to enhanced photoluminescence emission and local heating.

RESULTS AND DISCUSSION

The nanoantennas were prepared (for detail refer to the Methods) and arranged in a square lattice with the center to center distance between the patterns designed to be 2 μm (Figure 1A). A rectangular nanoantenna shape was preferred because their transverse and longitudinal surface plasmons can be selectively excited by the choice of the appropriate optical polarization. Next, we transferred large area CVD-grown MoS_2 monolayer films to these regions (for details of MoS_2 preparation and transfer refer to the Methods).[11] We inspect the photoluminance properties of these samples having in mind that the sample preparation procedure can diminish the interaction between the plasmonic and excitonic systems. This includes the limitations in achievement of perfect conformal contact between the two systems, polycrystallinity of the gold deposits, or variations in geometry of the antennas. A side view cartoon, demonstrating the general features of our samples, is depicted in Figure 1A. An optical image of typical hybrid MoS_2/Au antenna investigated in this work is shown in Figure 1B.

In order to first characterize the optical response of our nanoantennas we have performed elastic light scattering spectroscopy in the dark-field illumination mode. The polarization of the scattered light is analyzed in the parallel and perpendicular directions with respect to the antenna long axis. Typical polarization dependent light scattering spectra, acquired from a

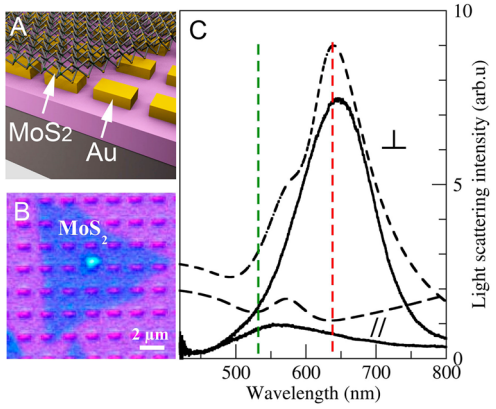

Figure 1. (A) Side view cartoon showing the general features of our samples. (B) Top view optical microscopy image (100× magnification) showing the region of MoS_2 coated and bare gold nanoantennas (100 × 1000 nm). The center-to-center distance between the gold nanoantennas (both in lateral and vertical directions) is 2 μm. (C) Simulated (dashed lines) and measured (solid lines) light scattering spectra of a single 100 × 1000 nm antenna in the spectral range of the transverse surface plasmon resonance. The polarization of the scattered light is analyzed in the directions parallel and perpendicular to the antenna long axis for an unpolarized excitation. The vertical dashed lines show the laser wavelengths used for photoluminescence excitation of MoS_2 out (532 nm) and in (638 nm) resonance with the transverse surface plasmons of the nanoantenna.

single 100 × 1000 nm bare nanoantenna, are shown in Figure 1C. The transverse surface plasmon resonance is clearly observed at 650 nm wavelength for scattered light polarization perpendicular to the nanoantenna long axis and vanishes for the parallel polarization. The good agreement between the polarization dependent spectra calculated using the GDM and the measured spectra confirms the wavelength range and the transverse character of the observed surface plasmon resonance. Throughout this study, we focus on the spectral range of the transverse surface plasmons because we are interested in the optical pumping of the MoS_2 photoluminescence *via* this plasmonic resonance. Indeed, since the MoS_2 photoluminescence (and absorption edge) is around 680 nm, the strongly red-shifted longitudinal surface plasmon resonance falls in the transparent region of MoS_2, whereas the transverse surface plasmon energy is above the MoS_2 band gap. In addition, shape imperfections, and in particular the rapidly increasing absorption of the titanium adhesion layer in the red and near-infrared spectral regions, lead to a strong damping of the longitudinal surface plasmon resonance.[12,13] As a matter of fact, in our shortest nanoantenna (100 × 300 nm), we could not observe the longitudinal surface plasmon resonance expected at 1200 nm according to the simulations. The transverse surface plasmon resonance (at 650 nm) falls in a spectral region of relatively moderate optical absorption of the titanium adhesion layer and are therefore weakly damped; moreover, for a fixed nanoantenna width (here 100 nm), the wavelength of the transverse

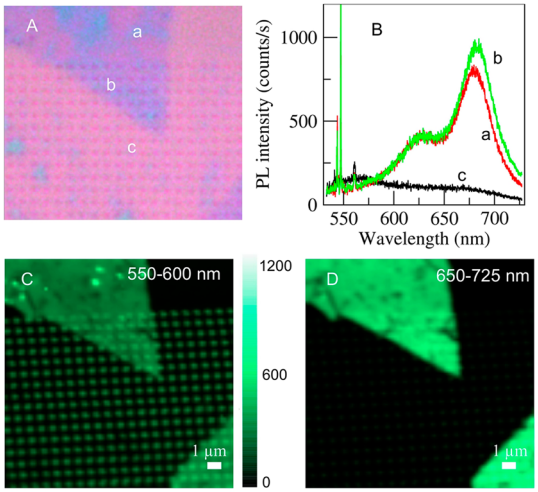

Figure 2. (A) Bright field optical microscopy image (100×) of the MoS_2 transferred to the 100 × 300 nm gold nanoantenna patterned substrate. (B) Photoluminescence spectra excited with the 532 nm laser line at different locations on the sample: MoS_2 on SiO_2/Si (a), MoS_2 on gold nanoantenna (b) and bare gold nanoantenna (c). (C and D) Photoluminescence intensity (in counts/s) maps spectrally integrated in the 550−600 nm and 650−725 nm range, respectively. The sharp lines are due to Raman scattering from the MoS_2 and from the Si substrate.

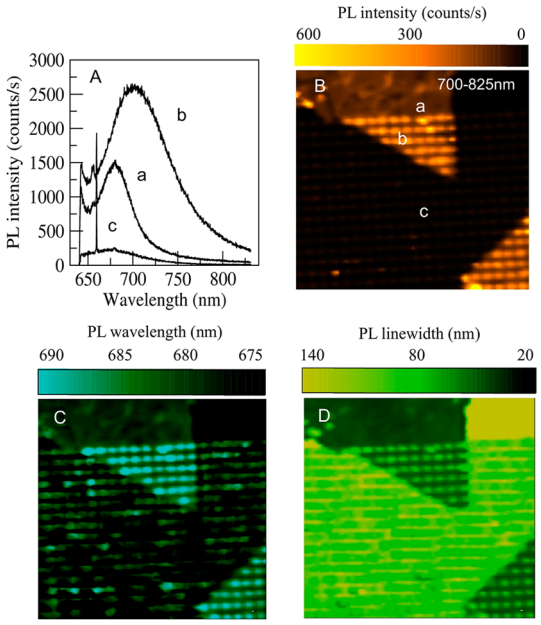

Figure 3. (A) Typical PL spectra recorded from MoS_2/SiO_2/Si (a), from MoS_2 on gold nanoantenna (b) and from bare gold nanoantenna (c). The sharp line is due to Raman scattering from the Si substrate. The PL intensity (B), wavelength (C), and line-width (D) maps were generated using a Lorentzian line shape fitting of the PL spectrum acquired at each point. The photoluminescence was excited at 638 nm close to the transverse surface plasmon resonance of the 100 × 300 nm nanoantenna with a laser intensity of 3 × 10^4 W/cm^2.

surface plasmon resonance does not depend on the length.[14] Indeed, light-scattering spectra, similar to those presented in Figure 1, have been recorded for all nanoantenna lengths (Figure S2, Supporting Information). A longer nanoantenna increases the optical volume for an unchanged transverse surface plasmon wavelength which may lead to more efficient light absorption and interaction with the MoS_2 layer as will be shown later. In addition, the elongated shape of the nanoantenna introduces an optical anisotropy that can be exploited for polarization selective excitation of the MoS_2 photoluminescence.

Figure 2 shows 100 × 300 nm gold patterns coated with MoS_2. As in Figure 1B, the MoS_2 layers also cover areas without nanoantennas providing three specific regions for sample characterization. These regions are MoS_2/SiO_2/Si (a), MoS_2/Au-antenna/SiO_2/Si (b), and Au/SiO_2/Si (c) as indicated in Figure 2A. Figure 2B displays the photoluminescence spectra recorded at selected points using a 532 nm laser excitation line with a spot size of approximately 350 nm (diffraction limited). The photoluminescence spectrum acquired from the bare nanoantenna (spectrum c) is broadened and much weaker than that of MoS_2 (spectra a and b). The PL spectrum of MoS_2 consists of two bands located at 625 and 680 nm which are due to radiative recombination of direct spin-split excitonic transitions.[1] The PL spectrum from the MoS_2/Au/SiO2/Si (spectrum b) is very similar to that of the MoS_2/SiO_2/Si (spectrum a) but it is slightly more intense due to the additional contribution from the gold nanoantenna. To better understand and acquire a statistical description of the MoS_2/Au coupling, we mapped the photoluminescence of the sample with a 300 nm step size (Figure 2C,D).

The PL intensity map generated using the 550−600 nm detection window (Figure 2C) clearly shows the emission from all the three regions of interest. In this wavelength range, the PL intensities from the pristine MoS_2, MoS_2/Au and the gold nanoantenna are comparable (Figure 2B). Conversely, in the 650−725 nm range the PL intensity of MoS_2 dominates and the bare nanoantennas are no longer visible (Figure 2D). In these first experiments, the excitation line (532 nm) is away from the transverse surface plasmon resonance (around 650 nm in Figure 1C) of the nanoantenna. We observe only tiny differences in the PL intensities from MoS_2 in and out of the nanoantenna regions. Moreover, we found no significant dependence of the PL signal on the incident polarization: the PL intensity is very similar for both polarizations parallel and perpendicular to the nanoantenna long axis. A clear signature of coupling between the MoS_2 layer and the surface plasmons can be further explored by using resonant excitation of the nanoantenna.

Figure 3 displays the PL spectra and maps obtained with an optical excitation at 638 nm, *i.e.*, close to resonance with the transverse surface plasmons of the nanoantenna. The laser intensity used in this study is 3 × 10^4 W/cm^2. Typical PL spectra (Figure 3A) acquired from the three distinct regions defined in

Figure 3B show major changes in the PL characteristics. A clear enhancement in PL intensity of MoS_2 on the nanoantenna region is observed (for polarization dependencies of these results refer to the Supporting Information, Figure S3). In addition, a red-shift and an increase of the line width are noticeable. To investigate this more accurately we acquire PL maps from these regions and fit the PL spectra using a Lorentzian line shape, thus generating PL peak intensity, wavelength, and line width maps as shown in Figure 3B–D. From these maps one can deduce that the photoluminescence of MoS_2/Au is systematically more intense, red-shifted, and broadened with respect to that of the $MoS_2/SiO_2/Si$ (Figure 3B–D). The collective observations here demonstrate an interaction between the excitonic transitions in MoS_2 and the surface plasmons of the gold nanoantennas. Better understanding of the observed characteristic changes is essential for their potential applications.

The enhanced PL intensity from the MoS_2/Au compared to $MoS_2/SiO_2/Si$ regions, by about ~65%, is a direct result of efficient optical absorption of the excitation light by the transverse surface plasmon of the nanoantenna (spectra b and c in Figure 3A). This exemplifies an important effect that can be utilized to increase to a great level the generally low absorption properties of these atomic layers and can be beneficial for many optoelectronic applications of MoS_2. Further evidence of plasmonic enhanced absorption is provided by the fact that the PL intensity is now strongly dependent on the incident polarization: the PL intensity of MoS_2/Au is nearly 4 times larger for laser polarization perpendicular to the nanoantenna long axis than for parallel polarization (Figure S3, Supporting Information); as a matter of fact, the longitudinal surface plasmons are strongly red-shifted (around 1200 nm for a 100 × 300 nm nanoantenna) with respect to the excitation line (638 nm) and are therefore not efficiently excited for parallel polarization. PL broadening and redshift are distinctive characteristic features of sample heating and the data presented in Figure 3 reveal a significant photoinduced heating.

In order to confirm our hypothesis about the origin of the PL broadening and redshift we studied the PL emission dependence on laser intensity. Since laser-induced heating is proportional to the intensity we anticipate a predictable change in both PL peak position and line width. Figure 4A shows the change in the PL spectrum of $MoS_2/SiO_2/Si$ as a function of laser intensity, increased from 3×10^2 W/cm^2 to 1.5×10^5 W/cm^2. Larger laser intensities initiate a rapid degradation of MoS_2 in accordance with previously reported studies.[15] As expected, the PL peak broadens and clearly red-shifts (inset of Figure 4A) with increasing laser intensity because of the optical absorption by the MoS_2 layer and the photoinduced local heating. This confirms that the increased absorption of the laser

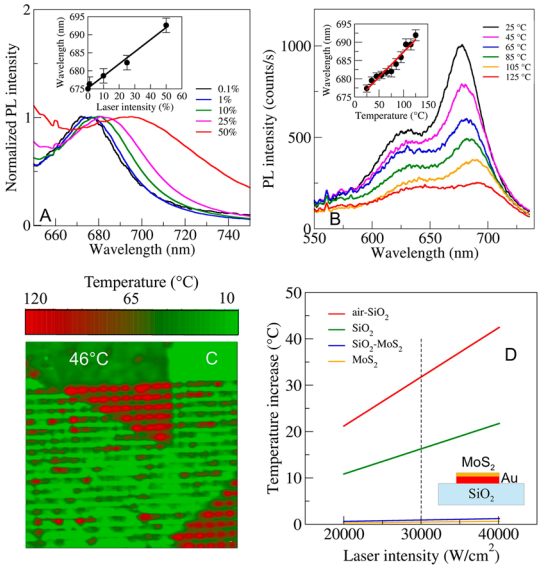

Figure 4. (A) Photoluminescence spectra of MoS_2 on SiO_2/Si excited at 638 nm with laser intensity increasing from 0.1% (3×10^2 W/cm^2) to 50% (1.5×10^5 W/cm^2) of the maximum value 3×10^5 W/cm^2. The laser polarization is perpendicular to the nanoantenna long axis. The inset shows the change of the emission peak wavelength. (B) Photoluminescence spectra of $MoS_2/SiO_2/Si$ excited at 532 nm with low laser intensity (3×10^2 W/cm^2) in order to minimize the laser-induced heating. The temperature of the sample holder is monitored up to 125 °C. The inset shows the change of the main emission peak wavelength with temperature; the red line is a linear least-square fit ($674 + 0.14 \times T$) nm. (C) Temperature map obtained by converting the PL peak wavelengths of Figure 3C to temperatures in °C. (D) Temperature increase as a function of laser intensity for various thermal conductivities of the surrounding medium (34.5 W/mK for MoS_2, 17.75 W/mK for SiO_2–MoS_2, 1 W/mK for SiO_2 and 0.512 W/mK for air–SiO_2). The dashed line shows the laser intensity at which the PL was excited.

light at the nanoantenna may cause local heating and thus broadening and redshift of the MoS_2 PL emission peak as observed in Figure 3. Next we calibrate the PL response to heating by measuring the $MoS_2/SiO_2/Si$ photoluminescence evolution from room temperature to 125 °C using a coldfinger optical microcryostat. In this case, the laser intensity has been maintained at a low value of 3×10^2 W/cm^2 in order to minimize the contribution of photoinduced heating. Figure 4B displays the temperature dependence of the PL spectra which clearly shows the broadening and redshift of the PL emission with increasing temperature. In particular, the A exciton peak with a wavelength around 680 nm increases linearly with temperature at a rate of (0.14 ± 0.01) nm/°C in agreement with previously published works).[16] The uncertainty in the PL peak wavelength is smaller than that of the peak line-width; this justifies the use of the PL peak wavelength rather than its width for temperature calibration. In addition, only the temperature dependence of the A exciton emission wavelength has been calibrated since the B exciton emission is very close to the excitation line (Figure 3) and the corresponding peak cannot be distinguished.

Once the temperature variation of the PL emission wavelength is calibrated, it is possible to convert the PL wavelength map displayed in Figure 3C into a temperature map as shown in Figure 4C. Obviously, the temperature values have no physical meaning in the regions where no MoS_2 layer is present. In the region where the MoS_2 is in contact with the SiO_2/Si substrate the estimated temperature is around 46 ± 10 °C. It is above room temperature because of the absorption by the MoS_2 layer and the subsequent photoinduced heating. As a matter of fact, the laser intensity (3×10^4 W/cm^2) used to excite the PL (Figure 3) is quite large and is responsible for a redshift of the PL emission wavelength as compared to the low-laser intensity excitation (Figure 4A,B). The precision on the temperature is determined by the uncertainty on the PL emission peak wavelength which we estimate around 3 nm given the relatively large PL line width. The most remarkable feature revealed in Figure 4 is that the MoS_2 temperature reaches 120 °C ± 20 °C above the nanoantenna array. Compared to the MoS_2/SiO_2/Si, the temperatures have risen by 74 °C. This temperature increase is attributed to the enhancement of the optical absorption due to the plasmonic resonance of the nanoantenna. It is important to delve deeper into the relationship between the temperatures measured using the MoS_2 PL emission wavelength and the plasmonic resonance of the gold nanoantenna and the mechanisms of heat generation.

Two main mechanisms can be invoked to explain the observed experiments: (i) The local electromagnetic field is strongly enhanced by the nanoantenna plasmonic resonance, thus giving rise to increased optical absorption into the MoS_2 layer as compared to MoS_2/SiO_2/Si. Before radiative recombination, the electron−hole pairs photogenerated in MoS_2 release their excess kinetic energy by phonon emission, thus leading to MoS_2 temperature increase. (ii) The resonantly excited surface plasmons of the nanoantenna may decay into electron−hole pairs inside the metal nanoparticle itself. The hot electron−hole gas generated in the Fermi sea may recombine radiatively which is responsible for the weak PL emission from the nanoantenna (Figure 3A, spectrum c); it may also relax its energy through electron−phonon interactions within the nanoantenna, which increases the nanoantenna temperature, thus producing a photothermal effect.[17] Then, the heat generated inside the nanoantenna diffuses and reaches the MoS_2 layer depending on the contact properties between the MoS_2 and the gold nanoantenna.

In order to distinguish between these two mechanisms, we have performed calculations of the heat generation and temperature elevation of the nanoantenna using the green dyadic method. The power dissipated in the nanoantenna can be deduced from the local electric field $E(r,\omega)$ in the metal (CGS units)[18]

$$Q(\omega) = \frac{\omega}{8\pi}\mathrm{Im}(\varepsilon_m(\omega))\int_V |E(r,\omega)|^2 \mathrm{d}r \qquad (1)$$

where V and $\varepsilon_m(\omega)$ are respectively the volume and the dielectric function of the gold particle.

We then determined the temperature elevation ΔT at the nanoantenna surface from the heat equation assuming a spherical heat source for simplicity.[10] One obtains $\Delta T = Q/4\pi a_{eq}\eta$[10] where a_{eq} is the radius of the spherical particle with equivalent nanoantenna volume and η is the thermal conductivity of the surrounding medium. As shown in ref 10, one important parameter for estimating the heat source is the deposited optical power, which strongly depends on the nanoparticle shape. It is here calculated using the GDM. Another other important parameter is the heat conductivity of the surrounding medium that determines the temperature at the nanoparticle surface. The nanoparticle shape has a little influence on the heat diffusion and release to the surrounding medium. That is why we assume a spherical heat source for which a simple solution of the Fourier equation can be derived.

Since the nanoantenna is in contact with the SiO_2 substrate and coated with MoS_2 we consider various situations for the thermal conductivity of the surrounding medium. The nanoantenna is fully surrounded either by SiO_2 (η = 1 W/mK) or by MoS_2 (η = 34.5 W/mK)[19] or by a medium having an average thermal conductivity (17.75 W/mK) in order to account for the heat loss through both the Au/SiO_2 and Au/MoS_2 interfaces. The situation of bare gold nanoantenna is also considered for comparison. In that last case, the SiO_2/air average thermal conductivity (η = 0.512 W/mK) is used.

For $I_{laser} = 3 \times 10^4$ W/cm^2, the maximum temperature increase is estimated around 32 °C and is obtained with the minimum SiO_2/air average thermal conductivity (Figure 4D). When the SiO_2/MoS_2 average thermal conductivity is used, which is more likely to describe the experimental situation, the temperature increase does not exceed 1 °C (Figure 4D). This value is much smaller than the measured temperatures that reach 120 °C above the nanoantennas (Figure 4C). Although very simple, the model used to evaluate the photoinduced temperature increase clearly indicates a weak contribution of the plasmonic absorption and subsequent heating of the gold nanoantenna (mechanism ii). Therefore, we may conclude that direct optical absorption, within the MoS_2 layer, enhanced by the strong plasmonic local electromagnetic field (mechanism i is responsible for more efficient electron−hole pair generation and thus for increased kinetic energy release and phonon emission). This is equivalent to the laser intensity effect shown in Figure 4A, where a larger amount of absorbed laser power leads to a photoinduced heating of the MoS_2 and a subsequent redshift of the PL signal. The PL intensity is also enhanced

(Figure 3B) due to the increased absorption by the MoS_2 layer.

Strictly speaking, PL intensity increase could be due to enhanced absorption and emission as both processes rely on the enhancement of the local optical density of states. Nevertheless, let us assume that there is enhancement of emission only. In that case, there is no reason for the strong PL redshift and broadening observed in Figure 3C,D. The latter require heating, and that is due to the increased number of photogenerated electron−hole pairs, *i.e.*, to increased optical absorption into the MoS_2. Moreover, it is well-known that PL emission could be quenched when the emitter is in the close vicinity of the plasmonic resonator.[20] Also, Bhanu *et al.*[21] have recently shown that the photoluminescence of MoS_2 flakes is strongly quenched upon Au deposition as a result of charge transfer from MoS_2 to Au. However, since in our experiments a PL enhancement of about 65% is measured (Figure 3B), we can conclude that increased optical absorption into the MoS_2 overpasses the PL quenching.

Since the near-field interaction between the MoS_2 layer and the plasmonic nanoantenna is at the origin of mechanism (i) we have calculated the plasmonic local field close to the nanoantenna surface using the GDM (Figure S4, Supporting Information). We found that the average enhancement factor of the electric field intensity $I = |E|^2$ is around 10 close to the bare nanoantenna surface (at the laser excitation wavelength and for a transverse polarization). Moreover, the absorbed optical power is proportional to the electric field intensity in the linear regime. Therefore, it is interesting to study the amount of optical power absorbed by each component of the hybrid system and how it is changing with the separation between the MoS_2 layer and the Au antenna. To do so, we have used the discrete dipole approximation (DDA)[22] to simulate the near-field interaction between a single MoS_2 layer and the Au antenna. We have calculated the optical powers absorbed by the Au antenna (mechanism (ii) and by the MoS_2 layer (mechanism (i) using

$$Q_{MoS_2(Au)} = \frac{\omega}{c} I \varepsilon''_{MoS_2(Au)} \int |E(r)/E_0|^2 dV_{MoS_2(Au)} \quad (2)$$

where E_0, ω, and I (in W/cm^2) are, respectively, the incident laser field amplitude, angular frequency, and intensity; $\varepsilon''_{MoS_2} = 7.9$ and $\varepsilon''_{Au} = 3$ are the imaginary parts of the dielectric constants (at the excitation wavelength) of a single layer MoS_2[23] and of bulk Au,[24] respectively. $E(r)$ is the calculated local electric field,[25] and the integrals run over either the MoS_2 or the Au volume.

As shown in Figure 5, for 1 nm MoS_2−Au separation, 32% of the absorbed power is due to the MoS_2 and 68% to the Au. The fraction absorbed by the MoS_2 is quite large despite its very small volume compared to that of the gold antenna. This is due to the

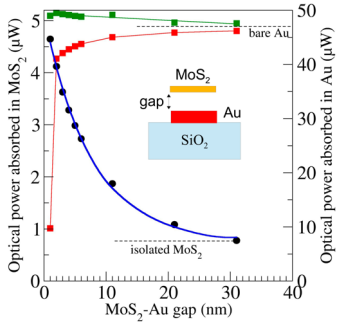

Figure 5. DDA calculations of the optical powers absorbed into MoS_2 (dots, left scale) and into Au (squares, right scale) as a function of the gap between the MoS2 single layer and the Au antenna surface. The incident laser intensity is 3×10^4 W/cm^2 (as in Figure 3 and 4C). The incident electric field is perpendicular to the antenna long axis and the wavelength is 638 nm. The blue curve is a fit of an exponentially decaying function $P(\mu W) = 0.77 + 4.35\ e^{-gap/7.6(nm)}$ to the numerical simulations. The red squares show the power absorbed in Au calculated with the actual dielectric constant of MoS_2 single layer. The green squares show the same calculations $\varepsilon''_{MoS_2} = 0$ with (*i.e.*, without absorption into MoS_2). In that case, the change in the power absorbed by the Au antenna is due to the detuning between the surface plasmons and the laser excitation. The horizontal dashed lines show the optical powers absorbed by an isolated MoS_2 single layer and by a bare Au antenna.

enhancement of the electric near-field in the vicinity of the antenna surface and to the larger absorption of MoS_2 compared to that of Au: $\varepsilon''_{MoS_2} = 2.64\varepsilon''_{Au}$. Because the electric near-field intensity weakens with increasing MoS_2−Au separation, the power absorbed by the MoS_2 layer decreases exponentially with a characteristic decay parameter of 7.6 nm (Figure 5). Conversely, the power absorbed by the Au antenna increases because the MoS_2 layer is more transparent (*i.e.*, less absorbing) and also because of the weaker surface plasmon damping due to the optical absorption into MoS_2. Indeed, weaker surface plasmon damping means larger electric near-field intensity and this is responsible for the initial rapid increase of the Au absorbed power that can be noticed in Figure 5.

Additionally, one more interesting piece of information that can be extracted from Figure 5 is the plasmonic enhancement factor of the MoS_2 absorption. Indeed, in comparison with the weakly interacting situation (30 nm MoS_2−Au separation) the absorbed power is increased by a factor 6 when the MoS_2 layer is located at 1 nm distance from the Au antenna surface. Hence, one may expect a similar factor for the PL intensity enhancement and temperature increase.

The measured PL intensity enhancement is only 65%. Several reasons could account for this difference. First, as shown in Figure 4B, the PL intensity dramatically decreases with increasing MoS_2 sample temperature. The fact that in the MoS_2−Au hybrid system the laser light is more efficiently absorbed is responsible both for enhanced PL emission but also for heating, which in turn decreases the PL intensity (Figure 4B).

Thus, plasmonic induced heating is a limiting factor for PL emission enhancement. Second, as discussed above, PL quenching is another limiting factor and is very likely to occur in our hybrid MoS_2−Au systems. The measured temperature increase ΔT (with respect to room temperature) is 4 times higher in MoS_2/Au than in MoS_2/SiO2/Si (Figure 4C) and is directly connected to the increase in optical absorption and density of photogenerated electron−hole pairs. In fact, we found a rather good agreement with the calculated enhancement factor 6 of the optical power absorbed in the MoS_2 layer (Figure 5), which confirms that the plasmonic enhancement of the MoS_2 layer optical absorption plays an important role and that mechanism i is responsible for the observed photoinduced heating (Figure 4). Finally, the calculated enhancement factor is certainly overestimated since the surface plasmons supported by the nanoantenna are damped because of shape imperfections, absorption in the Ti adhesion layer, and polycrystal gold obtained with e-beam lithography process.

CONCLUSION

In summary, we have reported the successful transfer of CVD grown MoS_2 monolayers to gold nanoantenna patterns synthesized using e-beam lithography. We have studied the photoluminescence emission from this hybrid system and identified the role of the plasmonic resonance. Using a systematic mapping of the photoluminescence signal, we found that for a resonant excitation of the surface plasmons, the photoluminescence of the MoS_2/Au layer is enhanced, broadened, and red-shifted with respect to that of MoS_2/SiO_2/Si. The enhancement of the PL emission is interpreted in terms of near-field interaction between the MoS_2 monolayer and the plasmonic resonator that leads to increased optical absorption and number of electron−hole pairs photogenerated into the MoS_2 layer. Broadening and red-shift of the PL emission is also attributed to laser-induced heating, a consequence of plasmonic enhanced optical absorption of the MoS_2 layer. By means of a careful calibration of the MoS_2 PL emission dependence on temperature, we were able to quantitatively characterize the surface plasmon effects in terms of local temperature increase. We found that the temperature rises by nearly a factor 4 due to the efficient absorption of the excitation light by the plasmonic resonance in agreement with DDA simulations. The presented work opens up a strategy for the engineering of plasmonic-based optoelectronic properties with the aim of enhancing the light-to-current conversion for applications in highly efficient photodetectors, highly sensitive biosensors, and plasmonic controlled field-effect transistors.

METHODS

To probe the plasmonic−excitonic and interaction in hybrid gold MoS_2/nanoantennas, rectangular resonators with varied aspect ratios were prepared using electron beam (e-beam) lithography. The nanoantennas are made of 4 and 36 nm thick evaporated titanium and gold, respectively. Titanium is used as an adhesion layer for better contact between the gold patterns and the SiO_2/Si substrate. Several morphologies were fabricated by maintaining a constant width of 100 nm and the length being systematically varied up to 1 μm.

The MoS_2 samples were prepared using a previously reported recipe in which MoO_3 powder is exposed to sulfur at elevated temperatures and a vapor-phase reaction leads to nucleation and growth of triangular single crystalline monolayers of MoS_2 on SiO2/Si substrates. Atomic force microscopy imaging was used to characterize the thickness of the MoS_2 layers (Figure S1, Supporting Information). Then, these substrates were coated with a PMMA film and suspended in KOH solution. After several cleaning steps with DI water the PMMA/MoS_2 was transferred to the gold nanoantenna. The PMMA is removed by acetone and the samples are annealed at 150 °C for 2 h in nitrogen environment.

Conflict of Interest: The authors declare no competing financial interest.

Acknowledgment. This work was supported by the computing facility center CALMIP of Paul Sabatier University of Toulouse. S.N. thanks LabEx NEXT for financial support under the "incoming PhD" mobility program. S.N. and J.L. also thank the support of Welch Foundation (Grant No. C-1716) and the NSF (Grant No. ECCS-1327093).

Supporting Information Available: AFM and height profile acquired from the monolayer MoS_2 samples that shows the thickness of typical samples in our measurements. Light-scattering spectrum acquired from a variety of gold nanoantenna aspect ratio designs showing the transverse surface plasmon. Photoluminescence intensity maps generated with 638 nm excitation, *i.e.*, close to the transverse surface plasmons of 100 × 400 nm Au antenna coated with MoS_2. Intensity enhancement map of the electric field at 20 nm above the surface of a100 nm × 300 nm antenna located on a SiO_2 substrate. This material is available free of charge *via* the Internet at http://pubs.acs.org.

REFERENCES AND NOTES

1. Mak, K. F.; Lee, C.; Hone, J.; Shan, J.; Heinz, T. F. Atomically Thin MoS_2: A New Direct-Gap Semiconductor. *Phys. Rev. Lett.* **2010**, *105*, 136805.
2. Lopez-Sanchez, O.; Lembke, D.; Kayci, M.; Radenovic, A.; Kis, A. Ultrasensitive Photodetectors Based on Monolayer MoS_2. *Nat. Nano.* **2013**, *8*, 497–501.
3. Zhu, Z. Y.; Cheng, Y. C.; Schwingenschlögl, U. Giant Spin-Orbit-induced Spin Splitting in Two-Dimensional Transition-Metal Dichalcogenide Semiconductors. *Phys. Rev. B* **2011**, *84*, 153402.
4. Zeng, H.; Dai, J.; Yao, W.; Xiao, D.; Cui, X. Valley Polarization in MoS_2 Monolayers by Optical Pumping. *Nat. Nano.* **2012**, *7*, 490–493.
5. Mak, K. F.; He, K.; Shan, J.; Heinz, T. F. Control of Valley Polarization in Monolayer MoS_2 by Optical Helicity. *Nat. Nano.* **2012**, *7*, 494–498.
6. Cao, T.; Wang, G.; Han, W.; Ye, H.; Zhu, C.; Shi, J.; Niu, Q.; Tan, P.; Wang, E.; Liu, B.; et al. Valley-selective Circular Dichroism of Monolayer Molybdenum Disulphide. *Nat. Commun.* **2012**, *3*, 887.
7. Lin, J.; Li, H.; Zhang, H.; Chen, W. Plasmonic Enhancement of Photocurrent in MoS_2 Field-Effect-Transistor. *Appl. Phys. Lett.* **2013**, *102*, 203109.

8. Goodfellow, K. M.; Beams, R.; Chakraborty, C.; Novotny, L.; Vamivakas, A. N. Integrated Nanophotonics Based on Nanowire Plasmons and Atomically Thin Material. *Optica* **2014**, *1*, 149–152.
9. Kang, Y.; Najmaei, S.; Liu, Z.; Bao, Y.; Wang, Y.; Zhu, X.; Halas, N. J.; Nordlander, P.; Ajayan, P. M.; Lou, J.; *et al.* Plasmonic Hot Electron Induced Structural Phase Transition in a MoS_2 Monolayer. *Adv. Mater.* **2014**, *26*, 6467–6471.
10. Baffou, G.; Quidant, R.; Girard, C. Heat Generation in Plasmonic Nanostructures: Influence of morphology. *Appl. Phys. Lett.* **2009**, *94*, 153109.
11. Najmaei, S.; Liu, Z.; Zhou, W.; Zou, X.; Shi, G.; Lei, S.; Yakobson, B. I.; Idrobo, J.-C.; Ajayan, P. M.; Lou, J. Vapour Phase Growth and Grain Boundary Structure of Molybdenum Disulphide Atomic Layers. *Nat. Mater.* **2013**, *12*, 754–759.
12. Jeppesen, C.; Mortensen, N. A.; Kristensen, A. The Effect of Ti and ITO Adhesion Layers on Gold Split-ring Resonators. *Appl. Phys. Lett.* **2010**, *97*, 263103.
13. Habteyes, T. G.; Dhuey, S.; Wood, E.; Gargas, D.; Cabrini, S.; Schuck, P. J.; Alivisatos, A. P.; Leone, S. R. Metallic Adhesion Layer Induced Plasmon Damping and Molecular Linker as a Nondamping Alternative. *ACS Nano* **2012**, *6*, 5702–5709.
14. Jain, P.; Huang, X.; El-Sayed, I.; El-Sayed, M. Review of Some Interesting Surface Plasmon Resonance-enhanced Properties of Noble Metal Nanoparticles and Their Applications to Biosystems. *Plasmonics* **2007**, *2*, 107–118.
15. Najmaei, S.; Ajayan, P. M.; Lou, J. Quantitative Analysis of the Temperature Dependency in Raman Active Vibrational Modes of Molybdenum Disulfide Atomic Layers. *Nanoscale* **2013**, *5*, 9758–9763.
16. Korn, T.; Heydrich, S.; Hirmer, M.; Schmutzler, J.; Schüller, C. Low-temperature Photocarrier Dynamics in Monolayer MoS_2. *Appl. Phys. Lett.* **2011**, *99*, 102109.
17. Thermo-Plasmonics: Using Metallic Nanostructures as Nanosources of Heat. *Laser Photonics Rev.* **2013**, *7*, 170−170.
18. Baffou, G.; Girard, C.; Quidant, R. Mapping Heat Origin in Plasmonic Structures. *Phys. Rev. Lett.* **2010**, *104*, 136805.
19. Yan, R.; Simpson, J. R.; Bertolazzi, S.; Brivio, J.; Watson, M.; Wu, X.; Kis, A.; Luo, T.; Hight Walker, A. R.; Xing, H. G. Thermal Conductivity of Monolayer Molybdenum Disulfide Obtained from Temperature-Dependent Raman Spectroscopy. *ACS Nano* **2013**, *8*, 986–993.
20. Goffard, J.; Gérard, D.; Miska, P.; Baudrion, A.-L.; Deturche, R.; Plain, J. Plasmonic Engineering of Spontaneous Emission From Silicon Nanocrystals. *Sci. Rep.* **2013**, 3.
21. Bhanu, U.; Islam, M. R.; Tetard, L.; Khondaker, S. I. Photoluminescence Quenching in Gold-MoS_2 Hybrid Nanoflakes. *Sci. Rep.* **2014**, 4.
22. Draine, B. T.; Flatau, P. J. Discrete-Dipole Approximation for Scattering Calculations. *JOSA A* **1994**, *11*, 1491–1499.
23. Yim, C.; O' Brien, M.; McEvoy, N.; Winters, S.; Mirza, I.; Lunney, J. G.; Duesberg, G. S. Investigation of The Optical Properties of MoS_2 Thin Films Using Spectroscopic Ellipsometry. *Appl. Phys. Lett.* **2014**, *104*, 103114.
24. Johnson, P. B.; Christy, R. W. Optical Constants of the Noble Metals. *Phys. Rev. B* **1972**, *6*, 4370–4379.
25. Flatau, P. J.; Draine, B. T. Fast Near Field Calculations in the Discrete Dipole Approximation for Regular Rectilinear Grids. *Opt. Express.* **2012**, *20*, 1247–1252.